A High-Power 4 × 4: Crystallographic and Electrochemical Insights into a Novel Wadsley-Roth Anode $Nb_9Ti_{1.5}W_{1.5}O_{30}$

Elizabeth Helen Driscoll,*[a,b,c] Alex Green [b,c], Dominic Fortes[d], Christopher Howard[d], Laura Louise Driscoll[b,c], Emma Kendrick[a,c], Colin Greaves[b], and Peter Raymond Slater *[b,c]

[a] School of Metallurgy and Materials, University of Birmingham, Edgbaston, B15 2SE, UK.

[b] School of Chemistry, University of Birmingham, Edgbaston, B15 2SE, UK.

[c] The Faraday Institution, Becquerel Avenue, Harwell, Didcot, OX11 0RA, UK.

[d] ISIS Neutron and Muon Source, Rutherford Appleton Laboratory, Harwell Campus, Didcot, OX11 0QX, UK.

Correspondence to:

Dr Elizabeth Driscoll and Prof. Peter Slater

The University of Birmingham,

Edgbaston,

B15 2TT,

UK

e.h.driscoll@bham.ac.uk

p.r.slater@bham.ac.uk

Experimental

Sample Preparation

The niobium titanium tungsten oxide materials were prepared through weighing stoichiometric amounts of Nb_2O_5, TiO_2 (anatase) and WO_3, which were then ground together using an agate pestle and mortar. The mixture was then heated up to 850°C/12hrs/5°C min^{-1} within an alumina crucible, and after intermittent grinding at room temperature, was re-heated up to 1100°C/12hrs/5°C min^{-1}.

Powder X-Ray Diffraction

The sample purity was evaluated using Powder X-ray Diffraction (PXRD), with the sample measured on an Empyrean PANalytical with a Cu tube (Kα). Pawley fits[1] to determine the unit cell made use of TOPAS software.[2,3]

Neutron Diffraction

Both samples were loaded into cylindrical vanadium foil containers of internal diameter 7.94 mm; the $Nb_9Ti_{1.5}W_{1.5}O_{30}$ sample holder was filled with 1.998 g of material to a depth of 24 mm. Neutron powder diffraction data were measured using the high-resolution instrument (HRPD) at the ISIS neutron spallation source.[4] The samples were mounted on a rotary sample changer installed in HRPD's sample vacuum tank and maintained under a rough vacuum (0.75 mbar) at room temperature.

Data were collected using HRPD's standard 30-130 ms time-of-flight (TOF) window, which results in diffraction data covering the *d*-spacing ranges from 0.65–2.60 Å in the instrument's highest resolution backscattering detectors (2θ = 158–176°; bank 1), 0.85–3.90 Å in the '90-degree' detectors (2θ = 80–100°; bank 2), and 2.3–10.2 Å in the forward-scattering detectors (2θ = 28–32°; bank 3). Data were collected for 2 h on each specimen, equivalent to 30 μA of proton-beam current. Reduction of the raw data was carried out with the Mantid suite of diffraction algorithms[5,6]; data were normalised to the incident spectrum and corrected for instrument efficiency using standard measurements of the empty instrument and of a null-scattering V:Nb rod. Absorption corrections were applied based on the calculated total scattering and absorption cross sections of the sample materials to thermal neutrons and the number density obtained from the mass and volume of the specimens as loaded. Data were then exported in a format suitable for analysis with GSAS.

Refinement

GSAS2-II[7] was used for structure refinement (with nuclear scattering lengths for W, Nb, Ti and O of 4.75, 7.05, -3.37and 5.81, all x10^{-15} m, respectively). Cation Bond Valence Sums were also provided by this program. Whereas Banks 1 and 2 were weighted at 1.0 in the refinements, Bank 3 was arbitrarily assigned a reduced weight of 0.25 to reflect its significantly lower intensity and resolution. The background was modelled using the Chebyschev-1 function, and the influence of preferred orientation was corrected using spherical harmonics.

SEM

The morphology was evaluated using Thermo Fisher Scientific Apreo 2 SEM in ETD mode, and elemental determination through an EDS detector. The accelerating voltage and probe current are provided on the given images.

Tap Density

Using Quantachrome Instrument AUTOTAP and applying a series of 1,000 taps to the sample, the sample's tap density was found to be 1.06 g cm^{-3}.

Cell Fabrication and Electrochemical Testing

To test the performance of the material as an anode, a slurry was produced with the following ratio: 80% active material: 10% binder: 10% conductive additive. The binder - polyvinylidene difluoride (PVDF) - was

mixed with N-methyl pyrrolidone (NMP) initially for 5 mins/1300 rpm, before additions of the Super P carbon black and the active material with subsequent additions of NMP to produce a slurry (10 mins/1300 rpm for each step). To degas the mixture, a final mix of 3 mins/1800 rpm was performed. The resulting slurry was cast onto copper foil using a draw-down coater, where the bar height was set to 200 µm. The resulting coating was dried for up to 2 hours at 80°C before being transferred for overnight drying in a vacuum oven pre-set at 110°C.

The AM electrode was cut to size (12 mm) before assembly. The AM – Li metal coin cells were assembled in an argon-filled glovebox. Steel 2032 cases were used, with a single 1 mm stainless steel spacer for compression. The lithium metal electrode was prepared from a dispensed fraction of lithium ribbon, where the surface was scratched using a stainless steel spatula (to remove the tarnished surface and leave a shiny and rough texture) before being cut to size (12.7 mm), ready for assembly. The electrolyte was 1.0 M LiPF6 in 50:50 (v/v) ethylene carbonate and dimethyl carbonate – two 50 µL 68 additions were made during assembly. The separator, glass fibre, was cut to size (14.3 mm). The active masses were found on average to be 4.1 (2) mg, giving an active mass coat weight of 3.4 - 3.82 mg cm^{-2}.

Cells were cycled between voltage limits of 1 V to 2.5 V. Initial formation cycling was conducted at 10 mA/g. More advanced rate testing was completed, and is outlined within the main body of the results and discussion. In addition to the constant current applied, a constant voltage step was applied on the lithiation step until a current breakdown of 40% of the original value was reached.

The method used in the rate testing (i.e. asymmetric currents) reduces potential lithium plating effects elevating the lithiation capacities, if the lithiation rate was to constantly increase.

Supporting Results

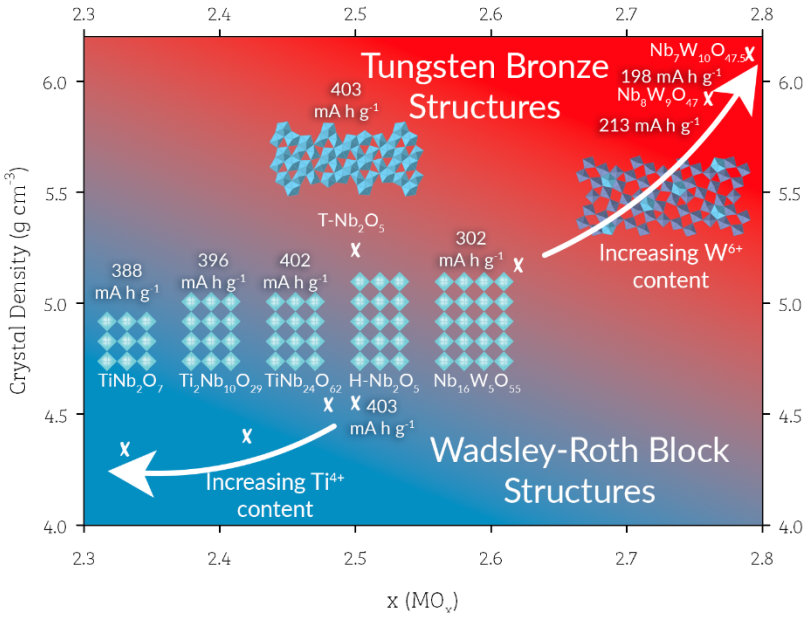

SI Figure 1: Schematic illustrating the crystal density vs MO_x (M = Nb, Ti, and W), with a multitude of WR structures with varying amounts of W^{6+} and Ti^{4+}.[8]

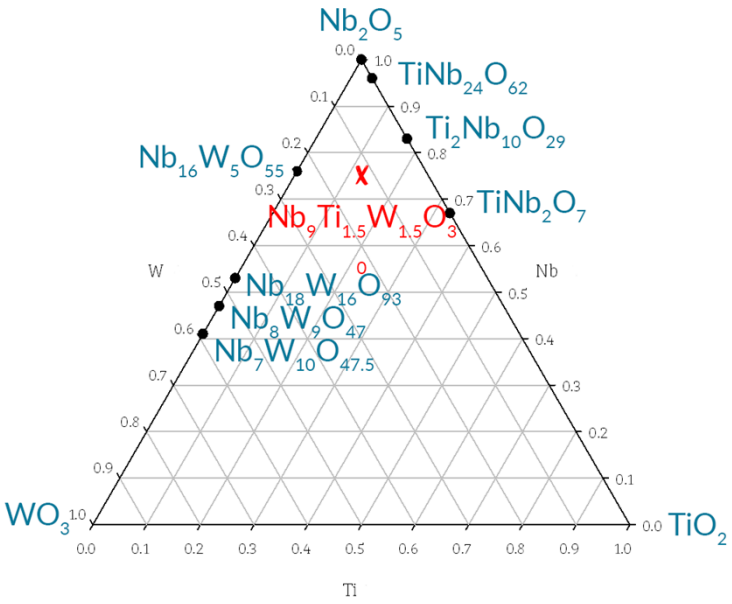

SI Figure 2: Ternary plot showing the proportion of each metal (Nb/Ti/W) for $MO_{2.5}$.[8]

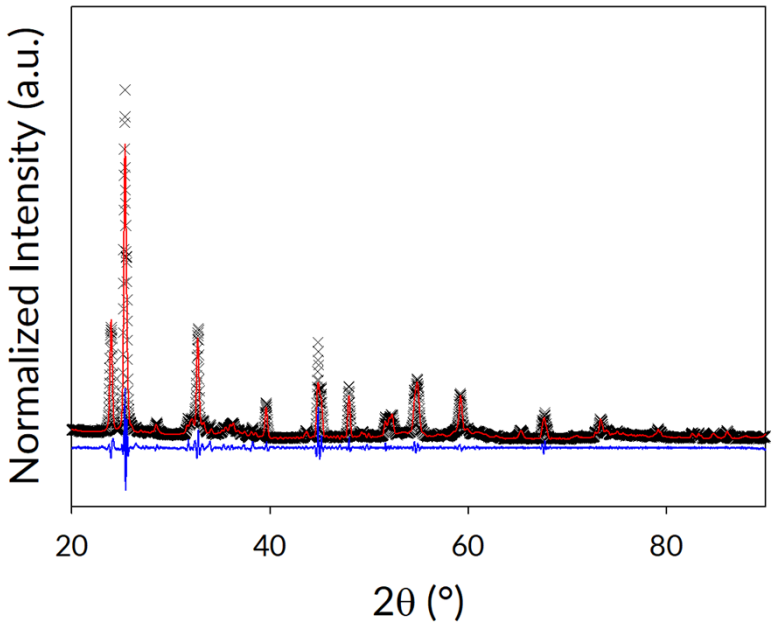

SI Figure 3: Observed, calculated and difference XRD profiles for $Nb_9Ti_{1.5}W_{1.5}O_{30}$ (Rwp – 7.87 %, Rp – 5.67%) (Cu Kα) – using C2/m symmetry and a Pawley fit.

The morphology of $Nb_9Ti_{1.5}W_{.15}O_{30}$ was observed to be rod-like as shown in SI Figure 4. This morphology is similar to what we have observed previously for the H-Nb_2O_5 phase[9]. The ratio of Nb:Ti:W from EDS is found to be 1: 0.17: 0.20 (1). As dispensed, to make this material, it is 1:0.17:0.17. Thus, W has not been lost on synthesis – given its volatile nature.

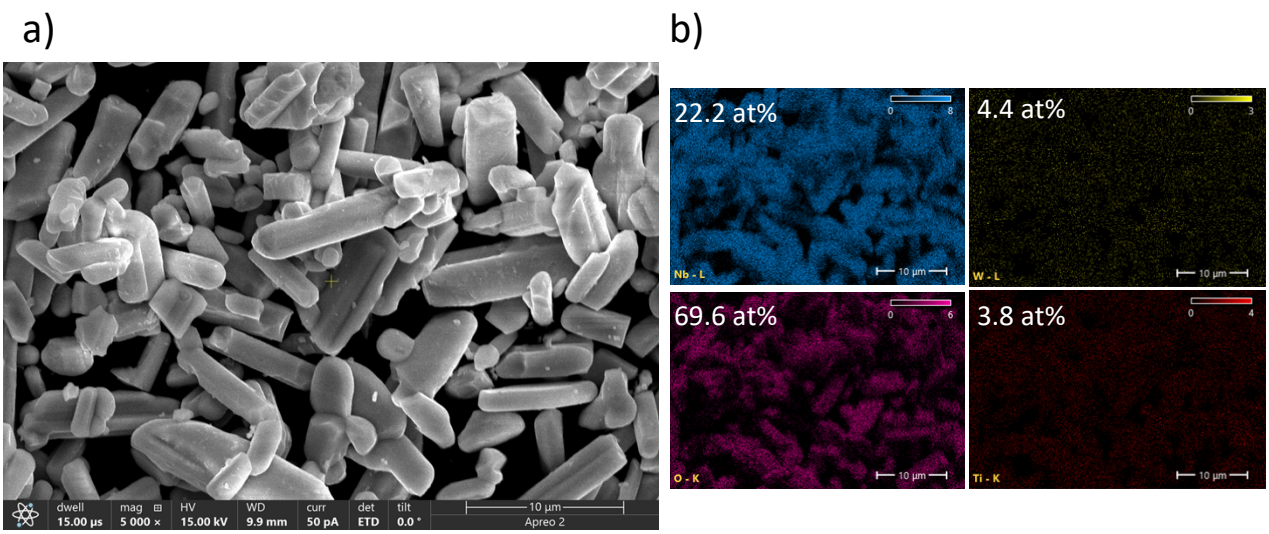

SI Figure 4: a) SEM image of $Nb_9Ti_{1.5}W_{1.5}O_{30}$ powder in the ETD mode, with the corresponding b) EDS maps of Nb, Ti, W, and O.

Initially, refinement assumed the composition as weighed out, and was based only on the NPD data in order to achieve precise locations for all atoms based on a random distribution of cations, giving an average site scattering length of 5.46×10^{-15} m, equivalent to a site occupancy of 0.77 Nb. The unit cell contains 24Nb, 4Ti, 4W and 80O. An additional benefit for this approach is that since Nb has the highest scattering length, refinement of the occupancies could indicate sites containing only Nb, and therefore an occupancy of 1.0 Nb. An iterative approach strongly suggested five Nb sites and three with a reduced occupancy which must contain one W and one Ti atom. The problem was therefore reduced to locating these two cations on the three sites, and the XRPD data was then included. The preferred solution was that one site was occupied fully by W, with the Ti distributed approximately evenly over the two remaining sites as shown in **Table 1** in the main paper. The negative scattering length of Ti resulted in site scattering lengths of 2.88 and 0.80 ($\times10^{-15}$ m) for NB/Ti1 and Nb/Ti2, respectively. Despite the incorporation of XRPD data, the reduced scattering at these sites is seen to give them higher esd values for their positional parameters. The fitted data for NPD Banks 2 & 3 and the XRPD data are shown in **SI Figure 4**, which provides residuals for each histogram. The overall residual for the four datasets was 5.5%.

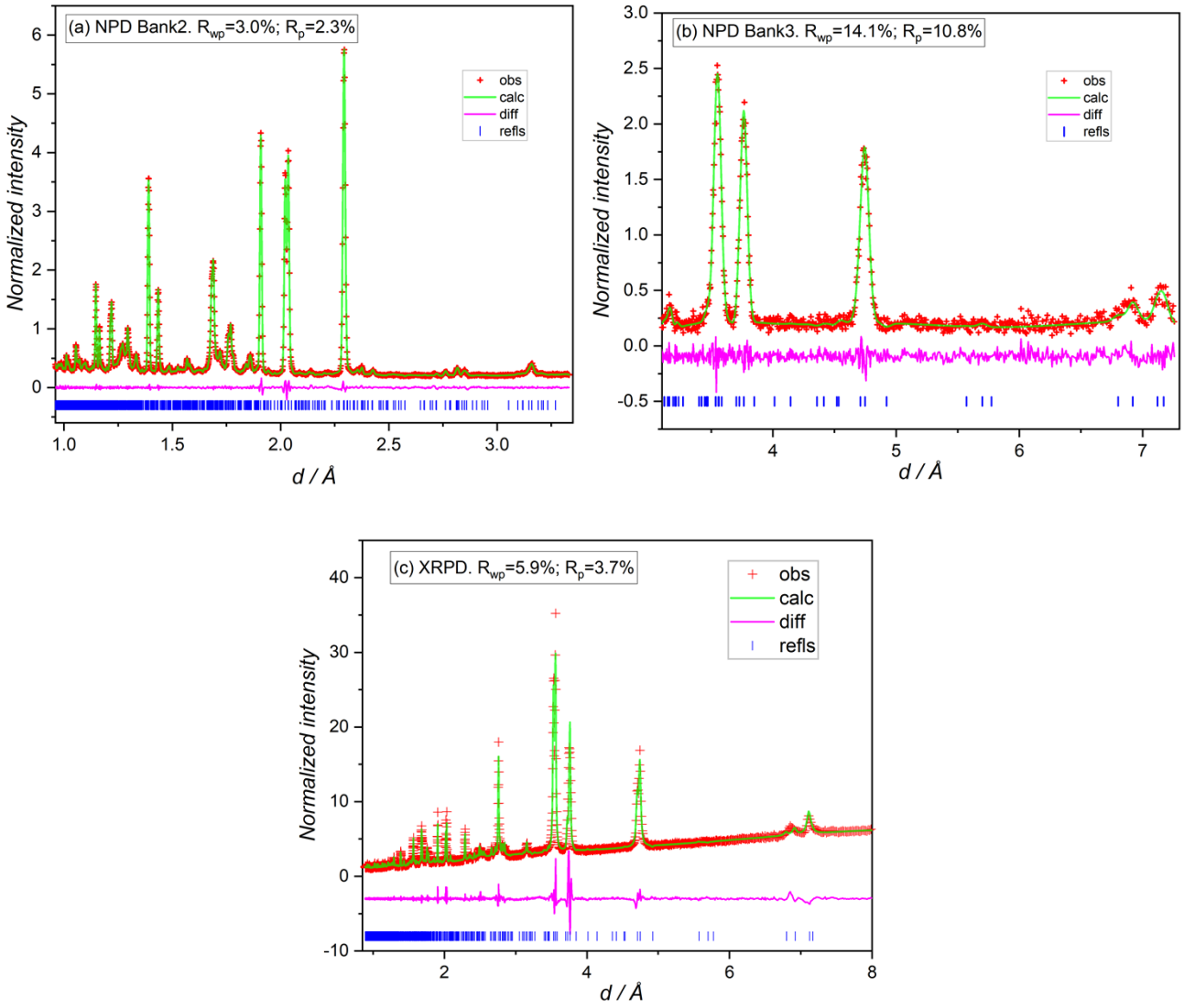

SI Figure 5: a) Bank 2 neutron diffraction data covering the d-spacing ranges from 0.85–3.90 Å in the '90-degree' detectors (2θ = 80–100°), and 2.3–10.2 Å in the forward-scattering detectors (2θ = 28–32°). b) Bank 3 neutron diffraction data covering the d-spacing ranges from 2.3–10.2 Å in the forward-scattering detectors (2θ = 28–32°), c) XRPD collected via PANalytical Empyrean.

SI Table 1: Structural Parameters from combined NPD/XRPD Rietveld refinement. All atoms in Site 4i, (x, 0, z). (Origin translated by (0, 0.5, 0) from reference [10].

Atom	*x/a*	*z/c*	*Occupancy*	$U_{iso} \times 100$ / Å^2
Nb1	0.2510(5)	0.3683(7)	1.0	2.5(1)
Nb2	0.3452(5)	0.6353(6)	1.0	2.5(1)
Nb3	0.3818(5)	0.3613(7)	1.0	2.5(1)
Nb4	0.4361(5)	0.1092(7)	1.0	2.5(1)
Nb5	0.5117(5)	0.3508(7)	1.0	2.5(1)
W1	0.1576(4)	0.1031(6)	1.0	2.5(1)
Nb/Ti1	0.2911(8)	0.105(1)	0.60(1)/0.40(1)	2.5(1)
Nb/Ti2	0.551(1)	0.060(1)	0.40(1)/0.60(1)	2.5(1)
O1	0.0193(5)	0.3645(7)	1.0	0.26(8)
O2	0.0636(5)	0.0807(7)	1.0	0.26(8)
O3	0.1238(5)	0.6475(7)	1.0	0.26(8)
O4	0.1756(5)	0.3662(7)	1.0	0.26(8)
O5	0.1954(5)	0.2125(8)	1.0	0.26(8)
O6	0.2110(5)	0.0879(7)	1.0	0.26(8)
O7	0.2633(5)	0.6380(7)	1.0	0.26(8)
O8	0.3051(5)	0.5126(7)	1.0	0.26(8)
O9	0.3100(4)	0.3535(7)	1.0	0.26(8)
O10	0.3332(4)	0.2257(7)	1.0	0.26(8)
O11	0.3519(5)	0.0769(7)	1.0	0.26(8)
O12	0.4258(5)	0.4893(7)	1.0	0.26(8)
O13	0.4549(5)	0.3683(7)	1.0	0.26(8)
O14	0.4872(5)	0.0663(7)	1.0	0.26(8)
O15	0.4734(4)	0.2211(6)	1.0	0.26(8)
O16	0.5908(5)	0.3658(7)	1.0	0.26(8)
O17	0.6109(5)	0.2451(7)	1.0	0.26(8)
O18	0.6300(5)	0.0710(7)	1.0	0.26(8)
O19	0.7783(5)	0.0818(7)	1.0	0.26(8)
O20	0.9091(5)	0.0478(7)	1.0	0.26(8)
Space Group C2/m; a = 28.289(4) Å, b = 3.8155(1) Å, c = 17.449(2) Å, β = 125.290(4)°, Vol = 1537.3(1) Å3; unit cell contents Nb24W4Ti4O80. Overall Rwp = 5.5%				

SI Table 2: Selected bond distances (Å) and Bond Valence Sums (BVS)

Nb1	- O4	2.11(2)	**Nb2**	- O4	1.992(5) ×2	**Nb3**	- O3	1.913(1) ×2
	O5	2.22(1)		O7	2.35(2)		O9	1.96(2)
	O7	1.940(3) ×2		O8	1.75(1)		O10	1.93(1)
	O8	2.06(1)		O16	1.82(2)		O12	1.82(1)
	O9	1.83(2)		O17	1.70(2)		O13	2.00(2)
BVS = 4.8			BVS = 6.5			BVS = 5.9		
Nb4	- O11	2.11(2)	**Nb5**	- O1	1.919(2) ×2	**W1**	- O5	1.56(1)
	O14	1.98(2)		O12	2.28(1)		O6	1.68(1)
	O15	1.60(1)		O13	1.80(2)		O18	2.014(4) ×2
	O20	2.104(6) ×2		O15	1.86(1)		O20	2.18(1)
				O16	2.10(2)			
BVS = 5.1			BVS = 5.4			BVS = 6.9		
Nb/Ti1	O6	2.11(1)	**Nb/Ti2**	- O2	1.938(4) ×2			
	O10	1.72(2)		O14	1.86(3)			
	O11	2.04(3)		O14	1.81(2)			
	O19	1.940(4) ×2		O18	2.14(3)			
BVS = 4.8(Nb); 3.7(Ti)			BVS = 4.9(Nb); 3.8(Ti)					

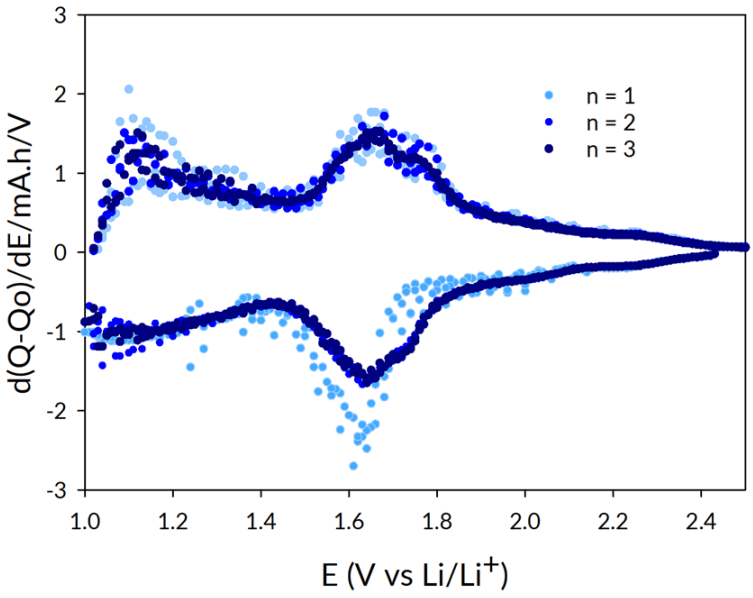

SI Figure 6: Differential specific capacity derived from the galvanostatic discharge/charge profile of $Nb_9Ti_{1.5}W_{1.5}O_{30}$.

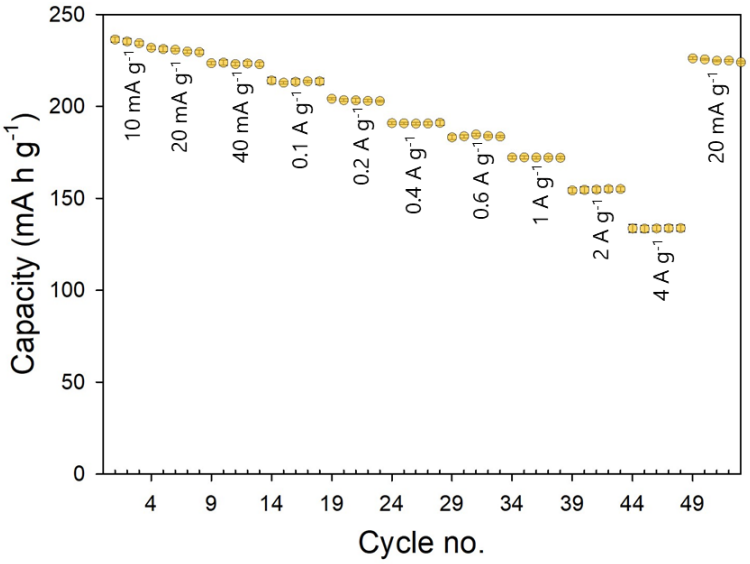

SI Figure 7: Resulting capacities of two cells undergoing rate testing, where the lithiation rate is increased and the delithiation rate is kept constant (reverse testing procedure to Figure 3b in the main manuscript).

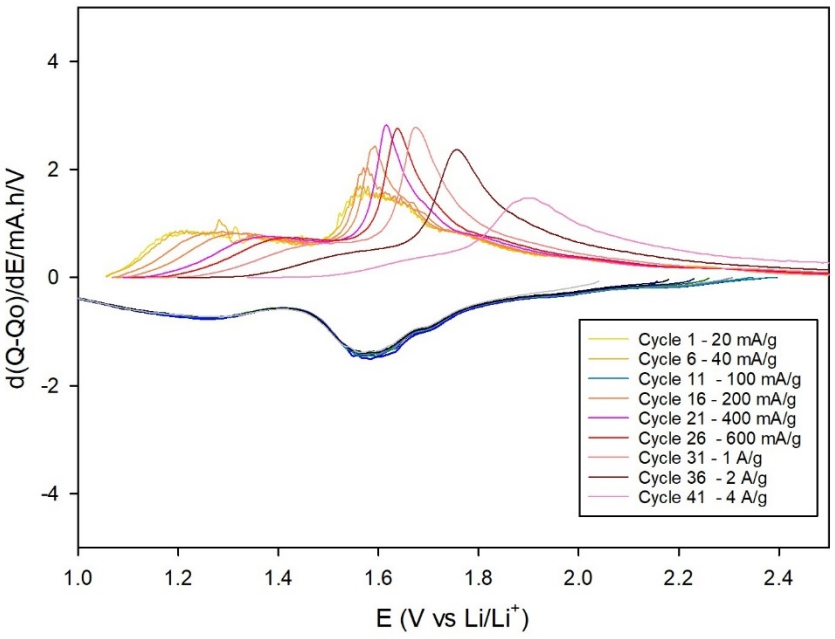

SI Figure 8: dq/dV plot derived from the galvanostatic discharge/charge profile of $Nb_9Ti_{1.5}W_{1.5}O_{30}$, where the delithiation rate was gradually increased from 20 mA g-1 up to a maximum of 4 A g-1, with the lithiation rate set as constant at 100 mA g^{-1}.

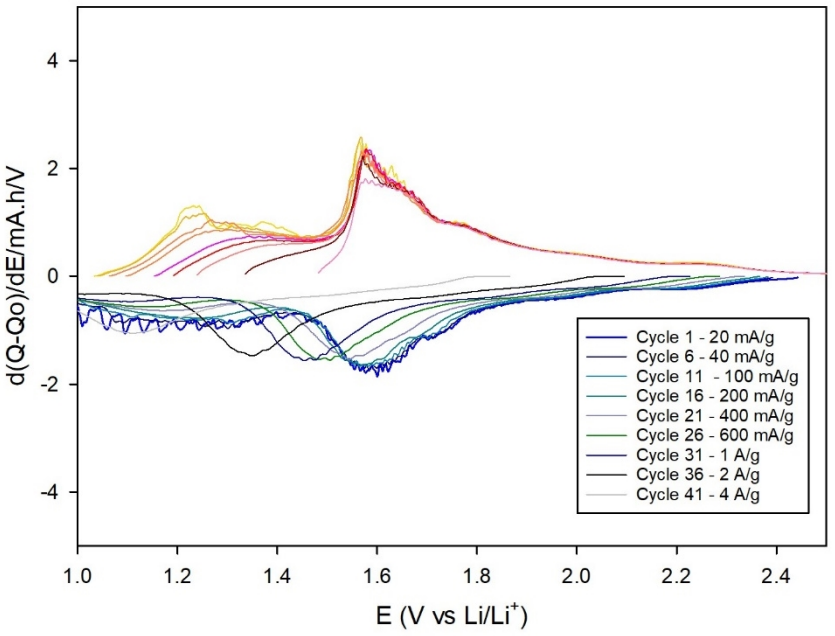

SI Figure 9: dq/dV plot derived from the galvanostatic discharge/charge profile of $Nb_9Ti_{1.5}W_{1.5}O_{30}$, where the lithiation rate was gradually increased from 20 mA g-1 up to a maximum of 4 A g-1, with the delithiation rate set as constant at 100 mA g^{-1}.

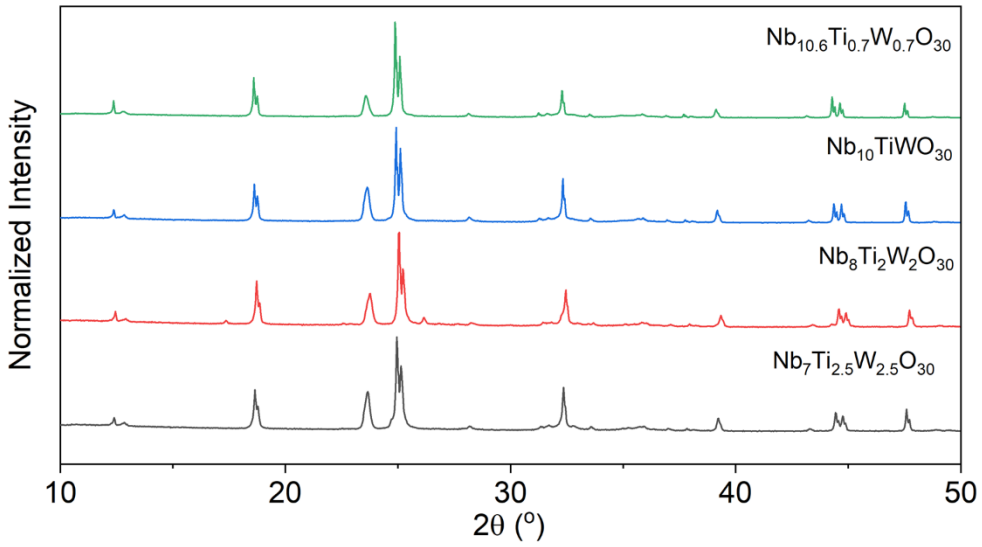

SI Figure 10: Resulting XRPD of a solid solution range of $Nb_{12-2x}Ti_xW_xO_{30}$ ($0.7 \leq x \leq 2.5$) (Cu Kα).

References

1 J. S. O. Evans, Pawley Fitting, https://community.dur.ac.uk/john.evans/topas_workshop/tutorial_tio2pawley.htm, (accessed 5 May 2022).

2 J. Perl, J. Shin, J. Schümann, B. Faddegon and H. Paganetti, *Med. Phys.*, 2012, **39**, 6818–6837.

3 B. Faddegon, J. Ramos-Méndez, J. Schuemann, A. McNamara, J. Shin, J. Perl and H. Paganetti, *Phys. Medica*, 2020, **72**, 114–121.

4 R. M. Ibberson, *Nucl. Instruments Methods Phys. Res. Sect. A Accel. Spectrometers, Detect. Assoc. Equip.*, 2009, **600**, 47–49.

5 O. Arnold, J. C. Bilheux, J. M. Borreguero, A. Buts, S. I. Campbell, L. Chapon, M. Doucet, N. Draper, R. Ferraz Leal, M. A. Gigg, V. E. Lynch, A. Markvardsen, D. J. Mikkelson, R. L. Mikkelson, R. Miller, K. Palmen, P. Parker, G. Passos, T. G. Perring, P. F. Peterson, S. Ren, M. A. Reuter, A. T. Savici, J. W. Taylor, R. J. Taylor, R. Tolchenov, W. Zhou and J. Zikovsky, *Nucl. Instruments Methods Phys. Res. Sect. A Accel. Spectrometers, Detect. Assoc. Equip.*, 2014, **764**, 156–166.

6 Mantid Project, Mantid (Manipulation and Analysis Toolkit for Instrument Data.; Mantid Project. http://dx.doi.org/10.5286/SOFTWARE/MANTID), ISIS Neutron and Muon Facility and Oak Ridge National Laboratory 2013.

7 B. H. Toby and R. B. Von Dreele, *J. Appl. Crystallogr.*, 2013, **46**, 544–549.

8 E. H. Driscoll, PhD thesis, University of Birmingham, 2022.

9 L. L. Driscoll, E. H. Driscoll, B. Dong, F. N. Sayed, J. N. Wilson, C. A. O'Keefe, D. J. Gardner, C. P. Grey, P. K. Allan, A. A. L. Michalchuk and P. R. Slater, *Energy Environ. Sci.*, 2023, **16**, 5196–5209.

10 S. Andersson, *ZAAC - J. Inorg. Gen. Chem.*, 1967, **351**, 106–112.